Macular Impairment in Fabry Disease: A Morpho-functional Assessment by Swept-Source OCT Angiography and Focal Electroretinography

Angelo Maria Minnella,[1,2] Lucilla Barbano,[3] Elena Verrecchia,[4] Francesco Martelli,[5] Valeria Pagliei,[1] Gloria Gambini,[1] Giorgio Placidi,[1] Benedetto Falsini,[1,2] Aldo Caporossi,[1,2] and Raffaele Manna[4]

[1]Institute of Ophthalmology, Università Cattolica del S. Cuore, Rome, Italy
[2]Fondazione Policlinico Universitario A. Gemelli IRCCS, Rome, Italy
[3]IRCCS- Fondazione Bietti, Rome, Italy
[4]Periodic Fever and Rare Diseases Research Centre, Università Cattolica del S. Cuore, Fondazione Policlinico Universitario A. Gemelli IRCCS, Rome, Italy
[5]Department of Cardiovascular, Dysmetabolic and Aging-associated Diseases, National Institute of Health, Rome, Italy

Correspondence: Lucilla Barbano, IRCCS- Fondazione Bietti, Via Livenza 3, Rome 00198, Italy; lucillabarbano@gmail.com.

Submitted: October 25, 2018
Accepted: May 24, 2019

Citation: Minnella AM, Barbano L, Verrecchia E, et al. Macular impairment in Fabry disease: a morpho-functional assessment by swept-source OCT angiography and focal electroretinography. *Invest Ophthalmol Vis Sci*. 2019;60:2667–2675. https://doi.org/10.1167/iovs.18-26052

Purpose. Fabry disease (FD) is a multiorgan X-linked condition characterized by a deficiency of the lysosomal enzyme *alpha-galactosidase A*, resulting in a progressive intralysosomal deposit of globotriaosylceramide. The aim of this study was to evaluate the macular ultrastructure of the vascular network using optical coherence tomography angiography (OCTA) and to evaluate macular function using focal electroretinography (fERG) in Fabry patients (FPs).

Methods. A total of 20 FPs (38 eyes, mean age 57 ± 2.12 SD, range of 27–80 years) and 17 healthy controls (27 eyes, mean age 45 years ± 20.50 SD, range of 24–65 years) were enrolled in the study. Color fundus photography, swept-source optical coherence tomography (SS-OCT), OCTA and fERG were performed in all subjects. The OCTA foveal avascular zone (FAZ), vasculature structure, superficial and deep retinal plexus densities (images of 4.5 × 4.5 mm) and fERG amplitudes were measured. Group differences were statistically assessed by Student's *t*-test and ANOVA.

Results. In the FP group, the FAZ areas of the superficial and deep plexuses were enlarged ($P = 0.036$, $t = 2.138$; $P < 0.001$, $t = -3.889$, respectively), the vessel density was increased in the superficial plexus, and the fERG amplitude was reduced ($P < 0.001$, $t = -10.647$) compared with those in healthy controls. No significant correlations were found between the structural and functional data.

Conclusions. OCTA vascular abnormalities and reduced fERG amplitudes indicate subclinical signs of microangiopathy with early retinal dysfunction in FPs. This study highlights the relevance of OCTA imaging analysis in the identification of abnormal macular vasculature as an ocular hallmark of FD.

Keywords: Fabry disease, retina, OCT angiography, focal electroretinogram, innovative biotechnology

Fabry disease (FD) (OMIM 301500) is a lysosomal storage disorder resulting from a deficient or absent activity of the lysosomal enzyme *alpha-galactosidase A*, which is encoded by the GLA gene on chromosome X (Xq22). This enzyme is involved in the degradation of glycosphingolipids, catalyzing the galactose terminal hydrolysis of globotriaosylceramide (GB3) by transforming it into lactosylceramide.[1–3] In the presence of GLA gene variants, the enzyme activity may be reduced or absent, thus leading to the progressive deposition of glycosphingolipids, including GB3, in various tissues, such as the vascular endothelium, kidneys, smooth muscle cells, and neuronal ganglions, resulting in subsequent cellular damage. The clinical presentation and disease severity may vary; although the onset of FD is often observed during childhood, it worsens during adulthood. Acroparesthesia, skin angiokeratomas, abdominal pain, fever, and anhidrosis or hypohidrosis are the most common symptoms in children. In adults, cardiac involvement with arrhythmias and left ventricular hypertrophy, cerebrovascular and renal dysfunction with proteinuria, and progressive kidney failure predominate the symptoms. An early diagnosis would lead to enzyme replacement therapy before any irreversible damage, thus reducing the risk of disease progression to organ failure.[4,5] The time of therapy as well as the individual response are important prognostic factors.

The ocular involvement in FD usually consists of corneal abnormalities, which present as cornea verticillata, lens opacity, and/or vascular abnormalities.[6,7]

Deposits of GB3 in the cornea take on a vortex pattern and are located in the corneal epithelium, basal and Bowman's membranes, and the anterior stroma, whereas they have not

Table 1. Genotype and Phenotype of the 20 FPs Included in the Study and the Corresponding Clinical Ocular Signs

Patient	Genotype	Phenotype	Ocular Signs
1	c.548G>C	Classical	Cornea verticillata, cataract, conjunctival and retinal vessel tortuosity
2	c.758T>C	Mild	Normal
3	c.907A>T	Mild	Conjunctival, eyelid rim, and retinal vessel tortuosity
4	c.644A>G	Late onset	Conjunctival, eyelid rim, and retinal vessel tortuosity, cataract
5	c.747C>A	Mild	Normal
6	c.758T>C	Classical	Conjunctival and retinal vessel tortuosity
7	IVS5+1G>T	Classical	Cataract, conjunctival and retinal vessel tortuosity
8	IVS5+1G>T	Classical	Cataract, conjunctival vessel tortuosity
9	IVS3+1G>A	Classical	Cornea verticillata, cataract, conjunctival and retinal vessel tortuosity
10	c.644A>G	Late onset	Conjunctival vessel tortuosity
11	c.548G>C	Classical	Cataract, conjunctival and retinal vessel tortuosity
12	c.548G>C	Mild	Cornea verticillata
13	c.644A>G	Late onset	Cornea verticillata, retinal vessel tortuosity
14	c.647 A>G	Late onset	Cataract, conjunctival and retinal vessel tortuosity
15	c.644A>G	Late onset	Cataract
16	c.730G>A	Classical	Cornea verticillata, conjunctival vessel tortuosity
17	c.644A>G	Late onset	Cornea "verticillata," conjunctival and retinal vessel tortuosity, cataract
18	c.747C>A	Mild	Conjunctival vessel tortuosity
19	c.548G>C	Mild	Normal
20	c.647 A>G	Classical	Cornea "verticillata," conjunctival and retinal vessel tortuosity, cataract

The phenotypes include classical (multiple, complete organ involvement), mild (incomplete organ involvement), and late onset (occurring in adult age or involving a single organ or system).

been demonstrated in the endothelium.[8,9] Anterior capsular and radial posterior subcapsular cataracts, increased tortuosity, or telangiectasia or small angiomas of conjunctival and retinal vessels are frequently observed.[10] Indeed, pathological deposits of GB3 in the vascular endothelium[11,12] may induce decreased vessel wall resistance to hydrostatic pressure, resulting in vascular tortuosity[13] and impaired tissue peripheral perfusion.[6,14]

These vascular abnormalities have been studied to date with color fundus photography and fluorescein angiography.[10]

The recent introduction of optical coherence tomography angiography (OCTA) enables the assessment of retinal and choroidal vascular flow features in several ocular vasculopathies without the injection of dye.[15] With the exception of a few reports (Hufendiek K, et al. *IOVS* 2018;59:ARVO E-Abstract 5460; Baur J, et al. *IOVS* 2018;59:ARVO E-Abstract 4249), little information regarding the use of OCTA in Fabry patients (FPs) is available in the literature. To our knowledge, the relationship between morphological retinal vascular changes in FD, which are described using OCTA, and their functional implication, as detected using focal electroretinography (fERG), has not yet been underlined. The aim of this study was to evaluate the superficial and deep capillary plexuses, the choriocapillaris and the foveal avascular zone (FAZ) using OCTA and to investigate macular function using fERG.

Methods

The study was conducted at the Institute of Ophthalmology, Università Cattolica del S. Cuore, Fondazione Policlinico Universitario A. Gemelli IRCCS, in Rome (Italy) in accordance with the principles of the Declaration of Helsinki.

The sample size of the study was preliminarily estimated by considering the results of a pilot series of measurements ($n = 10$) obtained in FPs, as well as in controls. Assuming a standard deviation of 20% for both the morphological and electrophysiological measurements, a total sample size of 36 subjects (20 FPs and 16 healthy controls) provided a power of 0.8, at a P value of less than 0.05, to detect a between-group difference of 25%.

A total of 20 patients (38 eyes) with a diagnosis of FD were enrolled between March 2017 and June 2017 (12 males and 8 females; mean age 57 ± 2.12 SD; age range of 27–80 years).

All patients were selected from a larger cohort ($n = 57$) that was followed by the Department of Periodic Fever and Rare Disease Research Centre of the same university. Recruitment was performed according to a collaboration between the two departments and following an internal procedure of ocular evaluation of FPs.

An age-matched group (mean age 45 ± 20.50 SD, ranging from 24 to 65 years) of 17 healthy subjects (10 males and 7 females), providing 27 eyes with no signs of any ocular disease, served as controls.

The essential requirement to be included in the study was an established diagnosis of FD demonstrated by performing an enzymatic assay, which was confirmed by genetic testing. FPs, aged 18 years or older, who were affected by different forms of the disease (classic, mild, and late onset), which were defined based on organ involvement and clinical features, were included in this study. Patients were evaluated globally, and disease severity was estimated using a severity score (Mainz severity score index) based on general, cardiological, nephrological, and neurologic involvement, which contributed to emphasizing the heterogeneity of the sample.[5] All data are summarized in Table 1.

The comorbidity of diabetes, atherosclerotic vasculopathy, glaucoma, or any other macular or retinal disorders was regarded as exclusion criteria. Similarly, patients with optical media opacity (lens opacity corresponding to a grading of > N1, C2, P1 in accordance with the lens opacities classification system 3)[16] and/or those who had an inability to maintain or difficulty maintaining visual fixation, which would have limited visualization of the retinal structure and execution of the functional examinations, were excluded from the study. Two eyes in the FPs were excluded due to severe optic media opacity (dense cataract C4) and retinal disorder (macular pucker) in accordance with the exclusion criteria of the study; among the controls, seven eyes were excluded because they presented with myopia or hyperopia >2 diopters (D). The remaining study eyes were emmetropic or slightly myopic (<1

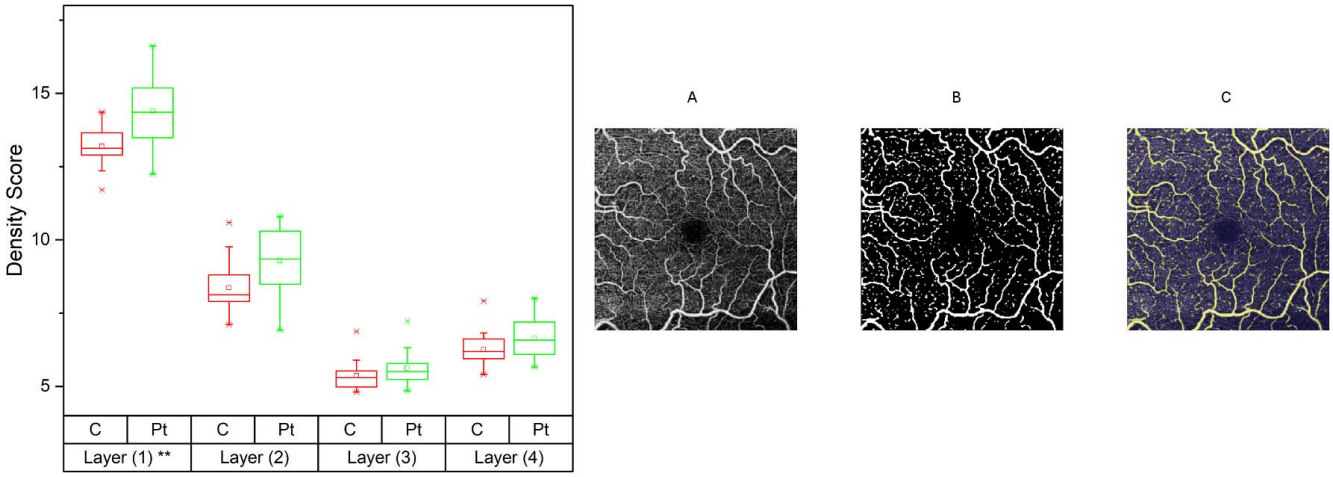

FIGURE 1. (*Left*) Density scores for the superficial vascular plexus (layer 1), deep capillary plexus (layer 2), outer retina (layer 3) and the choriocapillaris (layer 4) and subject type (Pt, patients; C, Controls) (** significant differences). (*Right*) OCTA images in a representative eye of a patient with FD: (**A**) original image; (**B**) detected superficial capillary layer (layer 1); (**C**) superimposition of images (**A**) and (**B**), with the numerical density score shown.

SPH D). Given such small refractive errors, axial length was not predicted to influence FAZ or vessel density measurements.

All patients underwent a full ophthalmological examination, including best corrected visual acuity (BCVA) and IOP measurements, as well as anterior segment slit lamp biomicroscopy and fundus ophthalmoscopy after pupil dilation with tropicamide 1% eye drops.

Color fundus images, structural OCT three-dimensional (3D) scans and OCTA 4.5 × 4.5-mm images were obtained using a DRI Triton Swept-Source OCTA device (Topcon, Tokyo, Japan). The quality of the B-scans was evaluated using the TopQ index provided by the device software. As far as OCTA, the quality was assessed on the basis of the mean value of the TopQ calculated as the average of the quality indexes of all the B-scans an OCTA image is composed of. Only scans provided with a TopQ >30 were retained for further analysis, and all the images and scans outside this limit were discarded.

The level of segmentation for each capillary plexus was automatically provided by the instrument: to detect the superficial capillary plexus, the upper segmentation line was situated at 2.6 μm under the inner limiting membrane, whereas the lower segmentation line was located 15.6 μm under the junction between the inner plexiform layer (IPL) and inner nuclear layer (INL). To identify the deep capillary plexus, segmentation lines were placed 15.6 μm under the junction between the IPL and INL and 70.2 μm under the junction between the IPL and INL. To detect the choriocapillaris, segmentation lines were positioned at the level of Bruch's membrane and 10.4 μm beneath it.

All B-scans were reviewed by two expert graders (AMM, LB) to exclude cases of failed segmentation. In cases of incorrect automatic segmentation, segmentation boundaries were manually adjusted. OCTA measurements of the FAZ area were performed by two investigators (AMM, LB) who were blinded to the clinical diagnosis, as well as to each other's findings. Spearman's rank-order correlation analysis was carried out. The agreement between the results of the investigators' analyses was satisfactory (correlation coefficient > 0.8). The FAZ area was manually calculated on the en face scans of the superficial and deep capillary plexuses.

The superficial and deep capillary plexus images were analyzed after applying the device proprietary projection artifact removal algorithm. OCTA scans (320 × 320 pixels, 24-bit RGB) of the superficial (layer 1) and deep capillary plexuses (layer 2) and of the outer retinal (layer 3) and choriocapillaris (layer 4) layers were checked for projection artifacts, computing 2D correlation coefficients between layers for each eye.[17,18] Scans with correlation coefficients greater than 0.25 (six FP eyes and one control eye) were discarded. Projection-free OCTA images of the 16 FPs (30 eyes, 120 images) and of the 10 age-matched healthy controls (19 eyes, 76 images) were selected for further analysis. The images were processed with a specifically developed algorithm, analogous to that reported by Kim et al.,[19] implemented in MATLAB (MathWorks, Inc., Natick, MA, USA) to compute a vascular density score for each image.

In detail, the following steps were performed:

1. The RGB images were converted to grayscale, eliminating the hue and saturation information while retaining the luminance, following International Telecommunication Union Recommendation BT.601.7,[20] Annex 2.
2. A modified version[21] of Niblack's algorithm[22] was used to remove uneven background luminance artifacts.
3. The image contrast was enhanced using histogram equalization.
4. Image binarization was performed following the method of Ridler and Calvard.[23]
5. Binary image morphological operations[24] (spur, majority, fill) were performed.

The density score was calculated as a ratio (expressed as a percentage) of the number of pixels of the corresponding vascular tissue to the total number of pixels in the image.[25]

Eight randomly chosen layer 1 angiographic images (four FPs, four controls; two right eyes and two left eyes for FPs and controls) were manually segmented by skilled operators (AMM, LB) to obtain a ground truth segmentation for comparison with the segmentation obtained using the algorithm.

A representative image of the eye of an FP that was analyzed with this system is shown in Figure 1.

fERG was performed as described in previously published works.[26] We assessed a monocular recording with an Ag-AgCl electrode taped on the skin over the lower eyelid after pupil dilation with tropicamide 1% eye drops. A similar electrode was placed over the eyelid of the contralateral patched eye and was used as a reference. Stimuli consisted of flickering uniform fields that were generated by an array of eight red light-emitting diodes (LEDs) covering an 18° diameter with a mean luminance

Clinical Findings	n° patients	Eye
Cornea verticillata (A)	7	OU
Increased tortuosity of conjunctival vessels (B)	14	OU
Increased tortuosity of eyelid rim	3	OU
Anterior or Posterior cataract	10	RE
Increased tortuosity of retinal vessels (C)	11	OU

Figure 2. Ophthalmological features of FD: (A, *top left*) cornea verticillata; (B, *top middle*) increased tortuosity of conjunctival vessels with angiomatosis and telangiectasia; (C, *top right*) increased tortuosity of retinal vessels. The table indicates the distribution of the listed ophthalmological signs in study patients. OU, both eyes; RE, right eye.

of 80 cd/m^2 and a temporal frequency of 41 Hz. The dominant wavelength of the stimulus was 630 nm. The flickering stimulus was sinusoidally produced by a custom-made digital frequency generator and presented on the rear of a modified Ganzfeld bowl (Primus; LACE Elettronica, Pisa, Italy) that was illuminated at the same mean luminance as the stimulus.

For the purpose of this study, we used a stimulation frequency of only 41 Hz. This frequency, under our experimental conditions, was optimal for the amplitude of the first harmonic component, as originally reported by Seiple et al.[27] and subsequently confirmed by our group.[28,29] In addition, it is well established that a 41-Hz flicker reflects the activity of both photoreceptors and bipolar cells.[28] A diffusing filter was placed in front of the LED array to make it appear as a circle of uniform red light. A steady DC signal maintained the mean luminance of the stimulus. A small square marker was placed in the center of the Ganzfeld bowl to allow steady fixation on the foveal region. The examined subjects were placed at a distance of 30 cm from the stimulus.

fERG signals were amplified, filtered (bandpass filter between 1 and 250 Hz), and averaged (12-bit resolution, 2-kHz sampling rate, 1600 repetitions in eight blocks). Signals exceeding the threshold voltage (25 mV) were rejected to minimize noise coming from blinks or eye movements. After the recording, a Fourier discrete analysis was performed to isolate the fERG first harmonic (1F), and its peak-to-peak amplitude was measured. Averaging and Fourier analyses also were performed on signals that were sampled asynchronously at 1.1 times the temporal frequency of the stimulus to estimate the background noise at the fundamental component. Under these conditions, the recorded fERG data were above the noise level (noise amplitude <0.08 mV in all cases) and were sufficiently reliable (the variation coefficient in amplitude was 20%).

For each patient and control, only the results from one eye (typically the right eye) were included in the statistical analysis; this was performed for all fERG and morphometric analyses for vascular density. Comparisons of the FAZ area and fERG amplitudes between patients and healthy controls were performed by independent two-tailed Student's *t*-tests. A P value less than 0.05 was considered statistically significant in all comparisons.

An independent samples *t*-test was conducted to compare the vascular density score in the images of both eyes of the FPs and controls.

A 2-way ANOVA with a post hoc Tukey test was conducted to compare the main effects of subject type (patient, control) and retinal layers (1, 2, 3, 4 as described above) on the density score. A $P < 0.01$ was chosen as the level of significance for this correlation.

In comparing FPs and controls, the potential for age bias was evaluated by testing the effect of age by linear regression analysis on morphometric and electrophysiological measurements. No significant effect of age was detected in the 40 to 60 age range; therefore, no correction for age was applied to the data.

Results

The mean BCVA among the 20 patients (38 eyes) who were diagnosed with FD and included in our study was 83 letters Early Treatment Diabetic Retinopathy Study (ETDRS) (corresponding to 0.04 logMAR) in the right eye and 84 (0.02 logMAR) in the left eye. The mean BCVA in the group of the healthy controls was 90 letters ETDRS in the right eye (–0.10 logMAR) and 92 in the left eye (–0.14 logMAR). For BCVA, no significant difference was found between the FPs and controls.

Among the prototypical findings of FD, cornea verticillata (Fig. 2A), increased tortuosity of the conjunctival vessels (Fig. 2B), increased tortuosity of vessels on the eyelid rim, anterior and posterior cortical opacity, and increased tortuosity of the retinal vessels (Fig. 2C) were observed in 7, 14, 3, 10, and 11 patients affected by the disease, respectively.

All patients in both groups had a normal IOP, a mean value of 13.5 mm Hg in FP and a mean of 13 mm Hg in controls. No alterations in macular thickness, morphology, and/or reflectivity were observed on OCT 3D scans in either FPs or controls.

In detail, a qualitative analysis of the OCTA scans showed a rarefaction of the superficial and deep retinal capillary plexuses, with the latter being more compromised, as a reduction in the blood flow in the perifoveal area (see also Fig. 6) was also noticed in the eyes of FPs compared to those of controls.

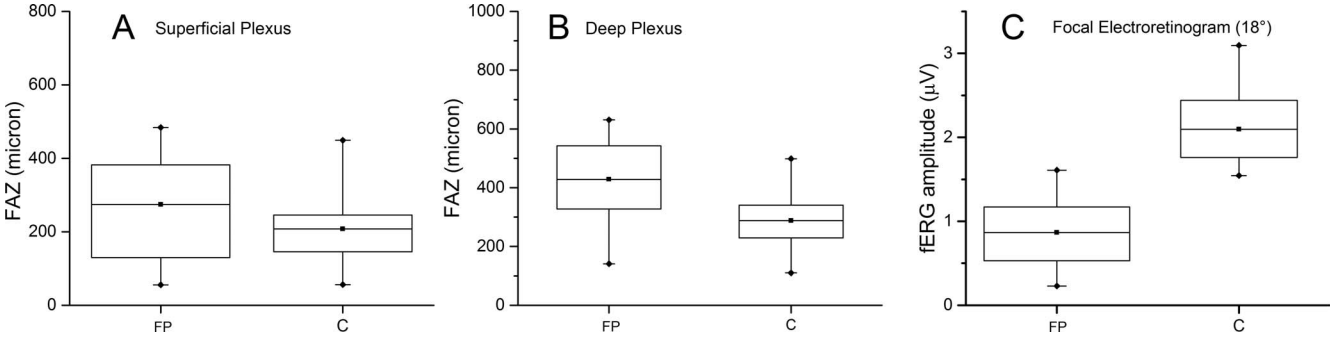

Figure 3. Boxplot representation of the FAZ measurements from the superficial (**A**) and deep (**B**) plexus and the fERG amplitude values (**C**) in eyes from an FP and a control (C).

As a further confirmation of these findings, manual measurement of the FAZ on the OCTA scans was carried out. The mean values of the FAZ areas on the superficial and deep capillary plexuses were 274.01 ± 137.62 SD and 428.69 ± 164.47 SD in FPs and 209.62 ± 98.16 SD and 288.04 ± 105.96 SD in controls. Further analysis of these data revealed a statistically significant enlargement of the FAZ; mean values for both the deep ($P < 0.001$, $t = -3.889$) and the superficial ($P < 0.05$, $t = 2.13$) vascular plexuses in the FP group compared to those in the control group (Figs. 3A, 3B).

fERG amplitude values (μV) obtained in FPs and in controls were 0.87 ± 0.41 SD and 2.22 ± 0.24 SD, respectively. A significantly lower fERG mean amplitude was found in FPs than in controls ($P < 0.001$, $t = -10.647$) (Fig. 3C), whereas the fERG phase did not show any significant differences between the groups (*t*-test not significant) (Fig. 4).

Although a trend toward an association between FAZ enlargement and reduction in fERG amplitude was noticed in the eyes of the FP group, no significant correlations between FAZ enlargement values and fERG amplitude or phase measurements were observed in the eyes of FPs (Fig. 5).

A vascular density score was computed for the superficial (layer 1) and deep capillary plexuses (layer 2), the outer retina (layer 3) layers, and the choriocapillaris (layer 4). The mean vascular density values in the FP group were 14.57 ± 1.10, 9.37 ± 1.02, 5.54 ± 0.51, and 6.69 ± 0.71 for layers 1, 2, 3, and 4, respectively. The vessel density values were 13.33 ± 0.59 (layer 1), 8.46 ± 1.00 (layer 2), 5.27 ± 0.38 (layer 3), and 6.40 ± 0.66 (layer 4) among the controls. No significant differences in the vascular density scores between the left (mean 8.91 ± 3.45 SD) and right (mean 8.90 ± 3.54 SD) eyes ($P = 0.93$; $t[55] = -0.09$) were found in the FP group.

The descriptive statistics of the computed density scores are reported in Table 2.

There was a statistically significant effect of the group on the vascular density score ($P < 0.001$; $F_{[1.96]} = 17.29$) as a result of a significant mean difference between the FPs (mean 9.04 ± 3.61 SD) and controls (mean = 8.36 ± 3.20 SD) (Table 3).

Table 2. Descriptive Statistics for Computed Vascular Density Scores in Control Eyes and FP Eyes Showing the Mean and SD Values

	Controls (10), Mean ± SD	Patients (16), Mean ± SD
Layer 1	13.33 ± 0.59	14.57 ± 1.10
Layer 2	8.46 ± 1.00	9.37 ± 1.02
Layer 3	5.27 ± 0.38	5.54 ± 0.51
Layer 4	6.40 ± 0.66	6.69 ± 0.71
All layers	8.36 ± 3.20	9.04 ± 3.61

Layers: superficial (layer 1), deep capillary plexuses (layer 2), outer retina (layer 3), and choriocapillaris (layer 4).

The main effect for the retinal layer yielded an *F* ratio of $F_{[3.96]} = 542.51$ ($P < 0.001$), indicating a significant effect of the retinal layer, as reported in Table 2. The interaction between groups (patients, controls) and retinal layer was not significant ($F_{[3.96]} = 2.19$, $P = 0.094$). Tukey's pairwise comparison test revealed a significant ($P < 0.01$) increase in the density score between the patients and controls in layer 1 (mean FD density increase =1.24) but not in layers 2, 3, or 4 (Table 4).

Segmentation algorithm performance was evaluated by comparing manually segmented images with those obtained with the binarization algorithm. The estimated algorithm sensibility and specificity were 0.68 (0.32 error margin) and 0.94 (0.17 error margin), respectively.

Assessment with the Spearman rank-order analysis showed no correlation between our results and the systemic severity of the disease quantified by calculating the Mainz severity score index.

Discussion

FD is characterized by the progressive accumulation of GB3 in any cell of the body, which leads to metabolic alterations and thus to cellular dysfunction. Several studies that have been performed in murine models have demonstrated that lysosomal deposits of GB3 may inhibit the receptors that are involved in the activation of the endothelial nitric oxide synthase enzyme, thus altering the vasoconstriction/vasodilation ratio of peripheral circulation with a consequent abnormal expression of endothelial K(Ca)3 channels.[12,13] These alterations are thought to be responsible for the development of vascular abnormalities, such as increased tortuosity, telangiectasis, and microaneurysms. These vascular features may involve several organs, such as the kidney, heart, and brain, leading to the development of renal failure, coronary dysfunction, and stroke, and they are thus responsible for the reduced life expectancy in FPs.[30–32]

Vascular alterations also may affect the eye and the retinal vasculature and may be related to retinal ischemia and its complications.[33–35] In our study, OCTA was used to investigate the vasculature features of FPs. A qualitative observation of a rarefaction of the retinal capillary plexuses, especially the deep capillary plexuses, suggests the presence of subclinical retinal ischemia, as previously found in several other retinal vasculopathies[36] (Fig. 6). Similarly, a significant enlargement in the FAZ implies a structural impairment of the macular area vasculature in this rare disease. These findings, however, were inconsistent with preserved visual acuity.

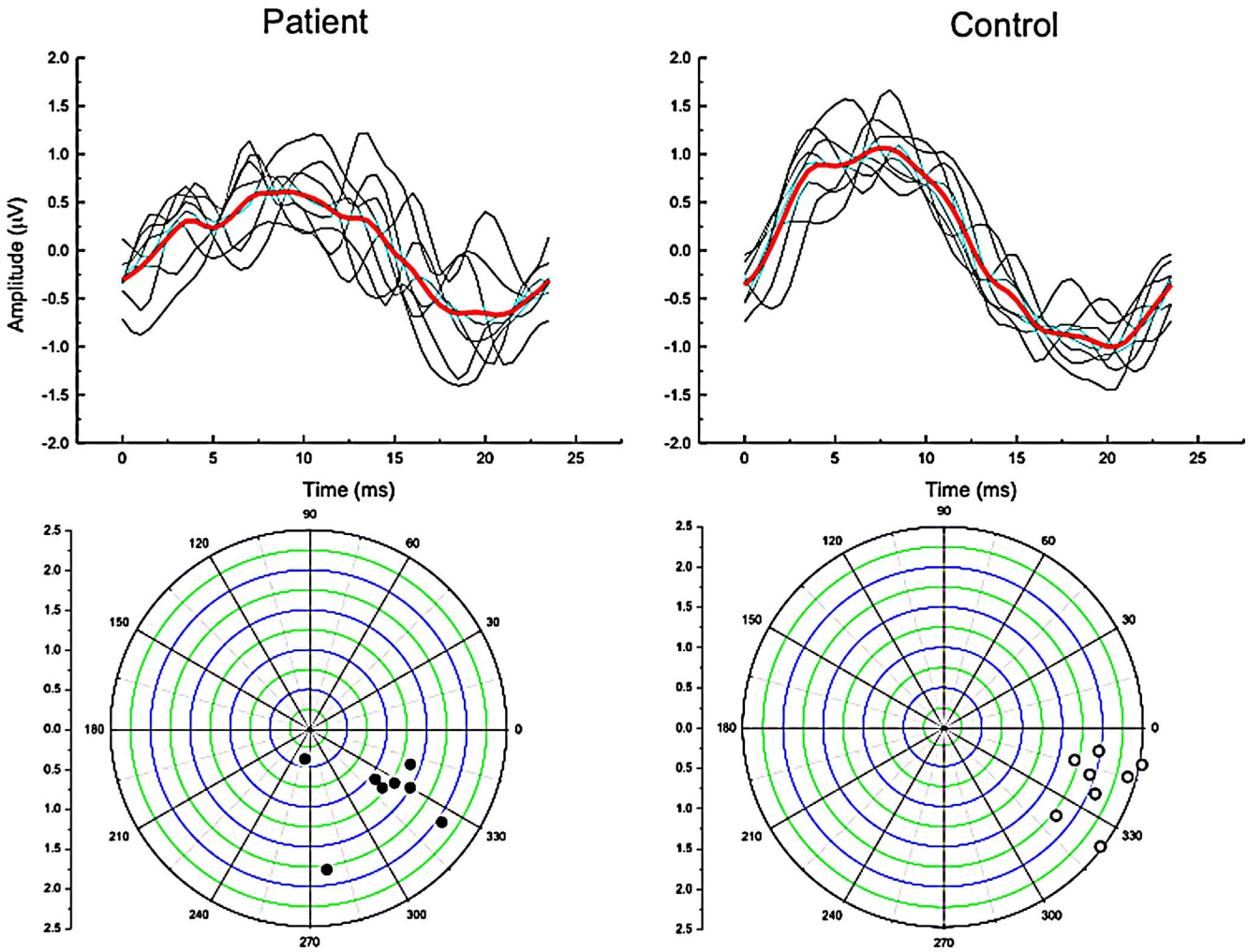

FIGURE 4. Representative examples of fERG recordings obtained from a typical FP and a control subject. On *top*, fERG tracings (eight blocks of responses) and their grand average (*red trace*) are shown. On the bottom, polar diagrams showing the response vector amplitude (in microvolts) and phase angle (in degrees) of the response fundamental harmonic (isolated by Fourier analysis) are reported. Note that the cluster of response vectors recorded from the FP eye show reduced amplitude (reduced vector length) compared with that from the control. Response phases (vector orientations) are similar between the representative patient and control.

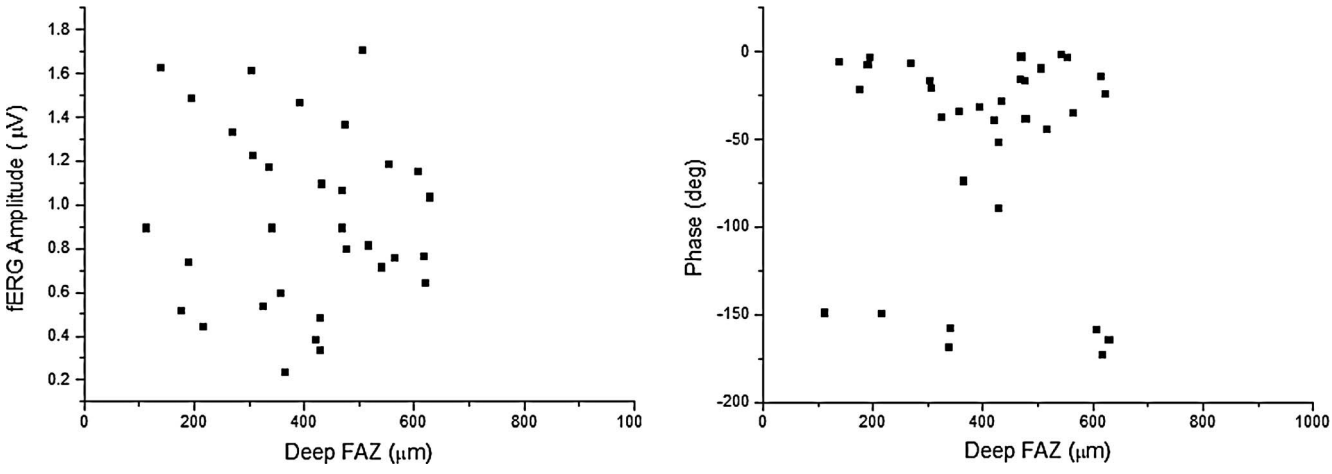

FIGURE 5. Scatterplot of fERG amplitude values as a function of the deep plexus FAZ: enlargement of the FAZ did not show a significant direct correlation with a reduction in the fERG amplitude (*Left*) or phase (*Right*). The data from both eyes are included in the figure.

Table 3. Two-way ANOVA That Was Computed for the Vascular Density Scores

Source of Variation	*df*	SS	MS	*F*	*P*
Subject type	1	**11.28**	**11.28**	**17.29**	**6.98E-0.5**
Retinal layer	3	**1062.15**	**354.05**	**542.51**	**0**
Interaction	3	4.28	1.43	2.19	0.09447
Model	7	1168.92	166.99	255.88	0
Error	96	62.65	0.65	–	–
Corrected total	103	1231.57	–	–	–

Subject type is patient or control. Significant effects are bold-faced. Alpha level = 0.01. df, degrees of freedom; MS, mean square; SS, sum of squares.

Consequently, the fERG method was used to further investigate the macular function to objectively assess the outer and middle retinal functional statuses. The deep capillary plexus is placed between the INL and the outer plexiform layer, where the bipolar cells are located and connected with photoreceptors. Evidence of a decreased fERG amplitude with preserved phase values in FPs suggests a subclinical dysfunction of the outer retinal layers.

All of these findings suggest that compromised vascular blood supply can harm photoreceptors and bipolar cells. However, no significant correlations were found between FAZ enlargement and fERG values, implying that, in addition to tissue perfusion deficits, other factors might be responsible for the observed abnormalities in outer retinal function.

For instance, the importance of the choriocapillaris layer in providing blood supply to the retinal pigment epithelium (RPE) and the photoreceptor layers should be considered, with a possible compensatory function of the more external ocular vasculature on the retina. Another possible reason for fERG abnormalities may be the accumulation of GB3 at the level of the RPE and photoreceptor cell membrane, similar to what occurs in the vascular endothelium, which may alter synaptic signaling between bipolar cells and photoreceptor cells. In fact, it is already known that lysosomal storage disorders may impair membrane trafficking.[37,38]

All of these hypotheses need to be verified by further histological or ultrastructural studies of the eyes from patients with this rare disorder.

fERG may show high test-retest variability[39] but also can be correlated with OCT parameters when a concomitant reduction in outer nuclear layer thickness occurs. This phenomenon is not the case for FD.

Automated measurements of vascular density scores of both the superficial and the deep capillary plexuses were obtained from an artifact-free subset of OCTA scans. FPs showed an increased vascular density in the superficial plexus in comparison with controls; this finding may be suggestive of vascular tortuosity, which represents a typical feature observed in FD.

The observation of FAZ enlargement associated with rarefaction of retinal capillary plexuses together with an increased vascular density may appear contradictory. However, because an increased vascular tortuosity may affect OCT signal reflectance, this outcome, in turn, may yield an increase in the density score (defined as the ratio between the area detected in the vessel and the total image area), even in cases with an enlarged FAZ area. In this view, an increase in the density score could be observed in subjects in whom expanded FAZ area suggests a general blood supply impairment.

An investigation of the vascular involvement in patients who are affected by FD was provided by the OCTA findings and represents a major strength of this study. Moreover, the combined use of OCTA to conduct a vascular structural analysis and fERG to assess retinal function provides an even deeper and more complete assessment. In this study, fERG can be regarded as a helpful tool in the identification of subclinical phases of FD, as supported by the fact that even in patients with a preclinical stage of FD, a reduction in fERG values was observed. In fact, two female FPs, whose medical conditions did not require any therapy, showed no signs other than a reduction in fERG amplitude. In our results, the decreased fERG amplitude is a statistically significant value that is worth considering.

The relatively small sample size is a major limitation of this study. A potential limitation to the study is the measurement of the eye's refraction and not the axial length; it is plausible that cataracts could change the lenticular contribution of refractive error to offset any axial length issues (i.e., a short eye with a myopic shift from the lens may be close to plano). Further clinical studies will validate OCTA and fERG as essential tools for the routine ophthalmological evaluation of patients who are affected by FD.

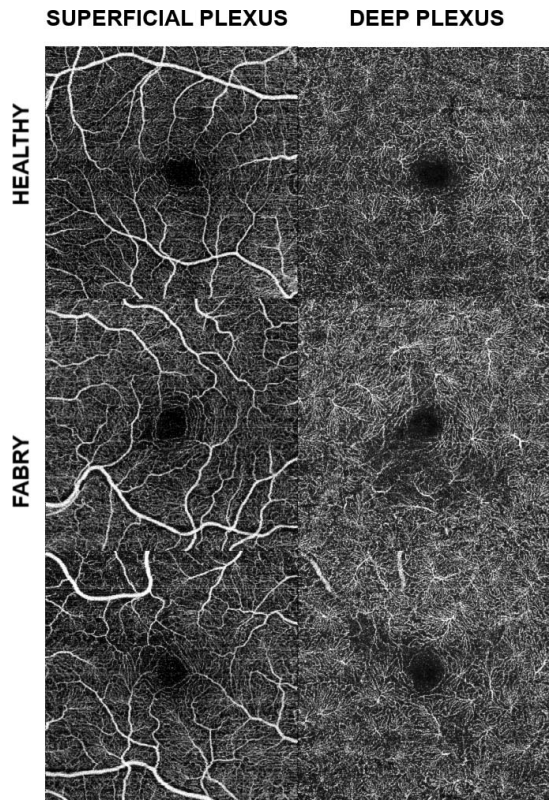

Figure 6. OCTA images of the superficial and deep capillary plexuses in the eyes of an FP and control, showing vascular tortuosity in the superficial plexus and a rarefaction-like ischemic area in the deep plexus of the eyes of the FP compared to those of the control.

Table 4. Tukey's Honestly Significant Difference Test Results of the Mean Vascular Density Score Differences (Patient Score − Control Score)

Retinal Layer	P − C Score	SEM	q Value	Prob	LCL	UCL
Layer 1	**1.24**	**0.33**	**5.38**	**0.01**	**0.05**	**2.42**
Layer 2	0.92	0.33	3.98	0.10	0.27	2.10
Layer 3	0.27	0.33	1.16	0.99	−0.92	1.45
Layer 4	0.28	0.33	1.24	0.99	−0.90	1.47

Significant effects are in bold; Alpha level = 0.01. P − C score, patient vascular density score − control vascular density score; Prob, probability; LCL, lower confidence limit; UCL, upper confidence limit.

Acknowledgments

Supported by the Ministry of Health and Fondazione Roma and Fondi di Ateneo linea D1, D3, Università Cattolica del S. Cuore (AMM, BF).

Disclosure: **A.M. Minnella**, None; **L. Barbano**, None; **E. Verrecchia**, None; **F. Martelli**, None; **V. Pagliei**, None; **G. Gambini**, None; **G. Placidi**, None; **B. Falsini**, None; **A. Caporossi**, None; **R. Manna**, None

References

1. El-Abassi R, Singhal D, England JD. Fabry's disease. *J Neurol Sci*. 2014;344:5–19.
2. Garman SC, Garboczi DN. The molecular defect leading to Fabry disease: structure of human alpha-galactosidase. *J Mol Biol*. 2004;337:319–335.
3. Dobrovolný R, Dvoráková L, Ledvinová J, et al. Recurrence of Fabry disease as a result of paternal germline mosaicism for alpha-galactosidase a gene mutation. *Am J Med Genet A*. 2005;134A:84–87.
4. Masson C, Cissé I, Simon V, Insalaco P, Audran M. Fabry disease: a review. *Joint Bone Spine*. 2004;71:381–383.
5. Whybra C, Kampmann C, Krummenauer F, et al. The Mainz Severity Score Index: a new instrument for quantifying the Anderson-Fabry disease phenotype, and the response of patients to enzyme replacement therapy. *Clin Genet*. 2004; 65:299–307.
6. Sivley MD. Fabry disease: a review of ophthalmic and systemic manifestations. *Optom Vis Sci*. 2013;90:e63–e78.
7. Sodi A, Ioannidis AS, Mehta A, Davey C, Beck M, Pitz S. Ocular manifestations of Fabry's disease: data from the Fabry Outcome Survey. *Br J Ophthalmol*. 2007;91:210–214.
8. Mastropasqua L, Nubile M, Lanzini M, Carpineto P, Toto L, Ciancaglini M. Corneal and conjunctival manifestations in Fabry disease: in vivo confocal microscopy study. *Am J Ophthalmol*. 2006;141:709–718.
9. Degirmenci C, Yilmaz SG, Onay H, et al. A novel mutation and in vivo confocal microscopic findings in Fabry disease. *Saudi J Ophthalmol*. 2017;31:45–47.
10. Dantas MA, Fonseca RA, Kaga T, Yannuzzi LA, Spaide RF. Retinal and choroidal vascular changes in heterozygous Fabry disease. *Retina*. 2001;21:87–89.
11. Satoh K. Globotriaosylceramide induces endothelial dysfunction in Fabry disease. *Arterioscler Thromb Vasc Biol*. 2014; 34:2–4.
12. Park S, Kim JA, Joo KY, et al. Globotriaosylceramide leads to K(Ca)3.1 channel dysfunction: a new insight into endothelial dysfunction in Fabry disease. *Cardiovasc Res*. 2011;89:290–299.
13. San Román I, Rodríguez M-E, Caporossi O, et al. Computer assisted retinal vessel tortuosity evaluation in novel mutation Fabry disease: towards new prognostic markers. *Retina*. 2017;37:592–603.
14. Tuttolomondo A, Pecoraro R, Simonetta I, Miceli S, Pinto A, Licata G. Anderson-Fabry disease: a multiorgan disease. *Curr Pharm Des*. 2013;19:5974–5996.
15. Spaide RF, Fujimoto JG, Waheed NK, Sadda SR, Staurenghi G. Optical coherence tomography angiography. *Prog Retin Eye Res*. 2018;64:1–55.
16. Chylack LT Jr, Wolfe JK, Singer DM, et al.; The Longitudinal Study of Cataract Study Group. The Lens Opacities Classification System III. *Arch Ophthalmol*. 1993;111:831–836.
17. Jonathan E, Enfield J, Leahy MJ. Correlation mapping method for generating microcirculation morphology from optical coherence tomography (OCT) intensity images. *J Biophotonics*. 2010;4:583–587.
18. Baran U, Choi WJ, Li Y, Wang RK. Tail artifact removal in OCT angiography images of rodent cortex. *J Biophotonics*. 2016; 10:1421–1429.
19. Kim T-H, Son T, Lu Y, Alam M, Yao X. Comparative optical coherence tomography angiography of wild-type and rd10 mouse retinas. *Trans Vis Sci Tech*. 2018;7(6):42.
20. International Telecommunication Union. *ITU recommendation BT.601–7 03 2011*. Geneva, Switzerland: International Telecommunication Union; 2011.
21. Sauvola J, Pietikäinen M. Adaptive document image binarization. *Pattern Recognit*. 2000;33:225–236.
22. Niblack W. *An Introduction to Digital Image Processing*. Englewood Cliffs: Prentice Hall; 1986.
23. Ridler T, Calvard S. Picture thresholding using an iterative selection method. *IEEE Trans Syst Man Cybern Syst*. 1978;8: 630–632.
24. Lam L, Lee S-W, Suen CY. Thinning methodologies-a comprehensive survey. *IEEE Trans Pattern Anal Mach Intell*. 1992; 14:869–885.
25. Jia Y, Bailey ST, Hwang TS, et al. Quantitative optical coherence tomography angiography of vascular abnormalities in the living human eye. *Proc Natl Acad Sci U S A*. 2015;112: E2395–E2402.
26. Abed E, Placidi G, Calandriello L, et al. Correlation of macular focal electroretinogram with ellipsoid zone extension in Stargardt disease. *J Ophthalmol*. 2017;2017:3643495.
27. Seiple WH, Siegel IM, Carr RE, Mayron C. Evaluating macular function using the focal ERG. *Invest Ophthalmol Vis Sci*. 1986;27:1123–1130.
28. Falsini B, Ziccardi L, Stifano G, et al. Temporal response properties of the macular cone system: effect of normal aging and age-related maculopathy. *Invest Ophthalmol Vis Sci*. 2007;48:4811–4817.
29. Falsini B, Iarossi G, Fadda A, et al. The fundamental and second harmonic of the photopic flicker electroretinogram: temporal frequency-dependent abnormalities in retinitis pigmentosa. *Clin Neurophysiol*. 1999;110:1554–1562.
30. Anastasakis A, Papatheodorou E, Steriotis AK. Fabry disease and cardiovascular involvement. *Curr Pharm Des*. 2013;19: 5997–6008.
31. Gubler M-C. Lésions rénales dans la maladie de Fabry [in French]. *La Revue de Médecine Interne*. 2010;31:S220–S225.

32. Moore DF, Kaneski CR, Askari H, Schiffmann R. The cerebral vasculopathy of Fabry disease. *J Neurol Sci*. 2007;257:258–263.
33. Sher NA, Reiff W, Letson RD, Desnick RJ. Central retinal artery occlusion complicating Fabry's disease. *Arch Ophthalmol*. 1978;96:815–817.
34. Abe H, Sakai T, Sawaguchi S, et al. Ischemic optic neuropathy in a female carrier with Fabry's disease. *Ophthalmologica*. 1992;205:83–88.
35. Pitz S, Grube-Einwald K, Renieri G, Reinke J. Subclinical optic neuropathy in Fabry disease. *Ophthalmic Genet*. 2009;30:165–171.
36. De Carlo TE, Romano A, Waheed NK, Duker JS. A review of optical coherence tomography angiography (OCTA). *Int J Retina Vitreous*. 2015;1:5.
37. Brogden G, Shammas H, Maalouf K, et al. Case study on the pathophysiology of Fabry disease: abnormalities of cellular membranes can be reversed by substrate reduction. *Biosci Rep*. 2017;37:BSR20160402.
38. Kuech E-M, Brogden G, Naim HY. Alterations in membrane trafficking and pathophysiological implications in lysosomal storage disorders. *Biochimie*. 2016;130:152–162.
39. Galli-Resta L, Piccardi M, Ziccardi L, et al. Early detection of central visual function decline in cone-rod dystrophy by the use of macular focal cone electroretinogram. *Invest Ophthalmol Vis Sci*. 2013;54:6560–6569.

Investigative Ophthalmology & Visual Science